Mijailovich et al., https://doi.org/10.1085/jgp.201611608

Normalization of the probability distributions of the attached states

The molecular origins of the differences in responses between different models for the same activation and mechanical protocols can also be explained by comparing the cross-bridge probability distributions. To compare the distributions between mass action models and MUSICO, it is necessary to determine the normalization factors that relate the state probability density functions, $p_i(x,t)$, in mass action models with the frequency of cross-bridges in each actomyosin state within a bin of the prescribed width, Δx_b, at the mean bin strain, x_b, from MUSICO simulations. The shape of the Duke model $p_i(x,t)$ is similar to the frequency distribution from MUSICO simulations only at early phases of force development when the number of bound cross-bridges is small. We derived the scaling factor in the following way: we fitted the frequency of attached cross-bridges per bin (Fig. S1, gray bars) by a modified Gaussian function (four parameters; Fig. S1, green line) and calculated the factor to match a peak of the fraction attached from Duke's mass action model (Fig. S1, black dashed line).

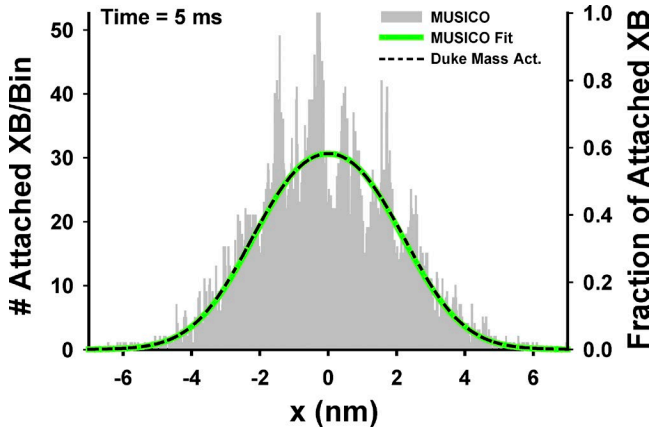

Figure S1. **Matching the scales of the number of attached cross-bridges per bin from MUSICO simulations to the fraction of attached cross-bridges from the Duke mass action model prediction at 5 ms after the onset of isometric force development.** The best fit of the number of attached cross-bridges (gray bars) by a modified Gaussian function (green line). The fraction of attached cross-bridges from the Duke mass action simulations (black dashed line) after matching the peaks almost perfectly aligns with the MUSICO predictions.

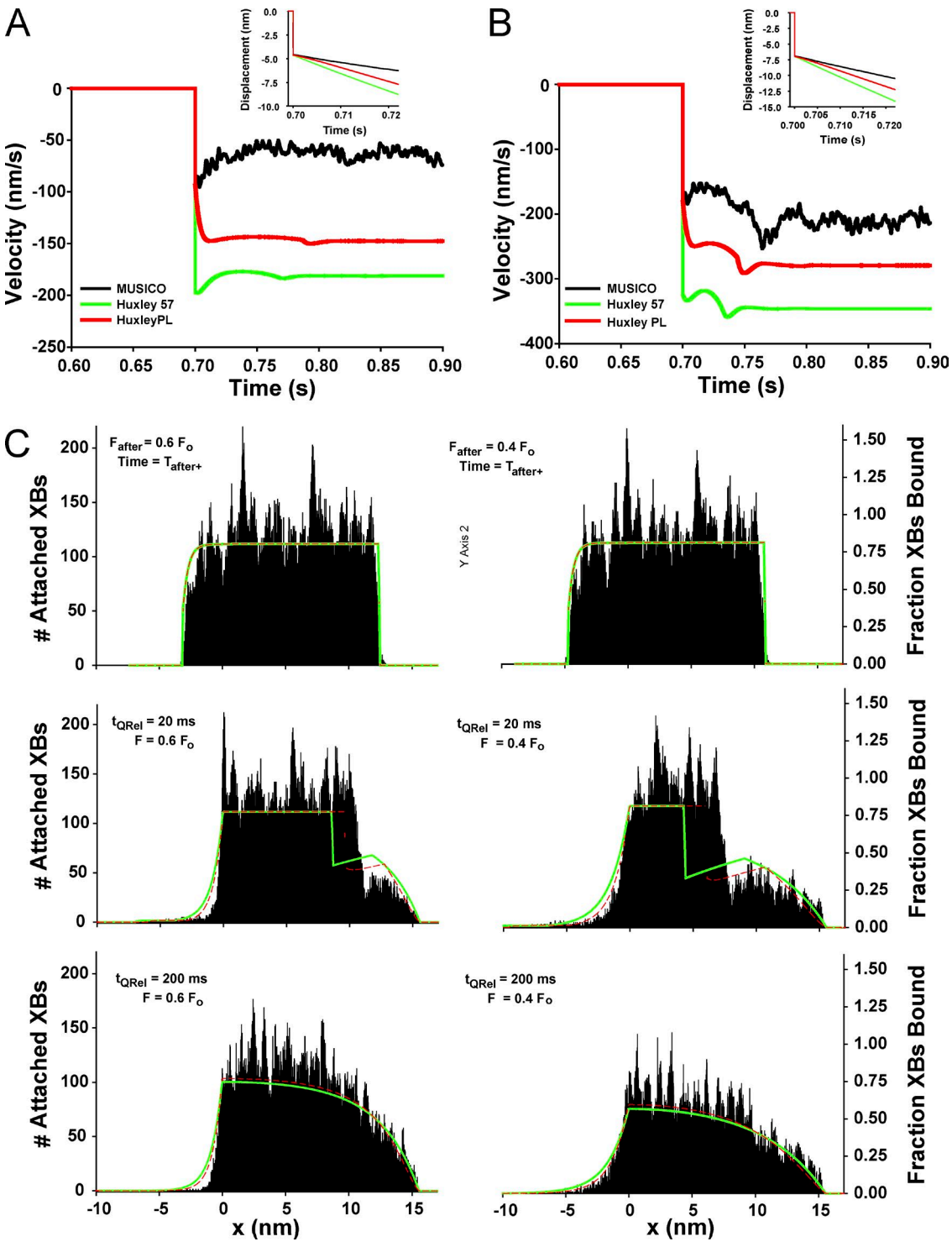

Figure S2. **Transient velocities and cross-bridge distributions after quick release to isotonic force at $F/F_o = T/T_o = 0.6$ and 0.4.** (A) Evolution of velocities after a quick release to an isotonic force of $F/F_o = T/T_o = 0.6$ predicted by MUSICO (black line), Huxley 1957 (green line), and Huxley PL (red line). The displacements after release are the same because the SE components of Huxley 1957 and Huxley PL models match the effect of the myosin and actin filaments from MUSICO (inset). (B) Velocity evolution after release to $F/F_o = T/T_o = 0.4$. (C) Cross-bridge distributions and state probability density distribution functions at times $t_{QRel} = 0_+$, 20, and 200 ms after release to $F/F_o = T/T_o = 0.6$ (left column) and to $F/F_o = T/T_o = 0.4$ (right column). Here black bars represent bound cross-bridges (MUSICO), bound cross-bridge distributions in the Huxley model are shown as solid green lines, and Huxley PL as dashed red lines.

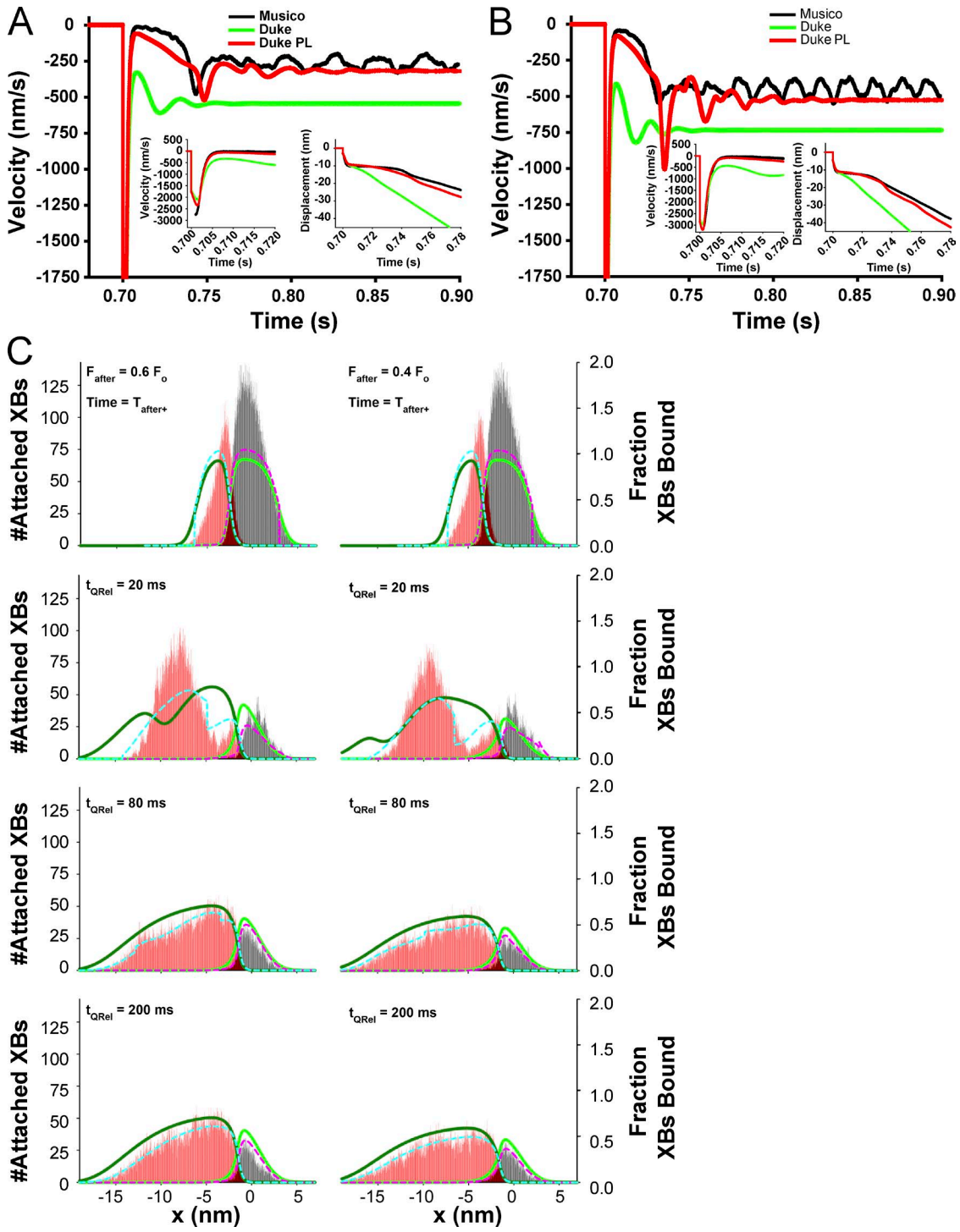

Figure S3. **Three-state model predictions of transient velocities and cross-bridge distributions after a quick release to isotonic force at $F/F_o = T/T_o = 0.6$ and 0.4.** (A) Evolution of velocities after a quick release to isotonic force of $F/F_o = 0.6$ predicted by MUSICO (black line), Duke (green line), and Duke PL (red line). The displacements after release are the same because the SE components of Duke and Duke PL models match the effect of the myosin and actin filaments from MUSICO (inset). (B) Velocity evolution after release to at $F/F_o = 0.4$. (C) Cross-bridge distributions at times $t_{QRel} = 0_+$, 20, and 200 ms after release to $F/F_o = T/T_o = 0.6$ (left column) and to $F/F_o = T/T_o = 0.4$ (right column), where black bars represent weakly bound cross-bridges and red bars the post-power stroke bound myosins (MUSICO). Duke state probability density distribution functions are shown as solid lines (weakly bound as a green line and post-power stroke a dark green line) and Duke PL as dashed lines (pink and cyan, respectively).

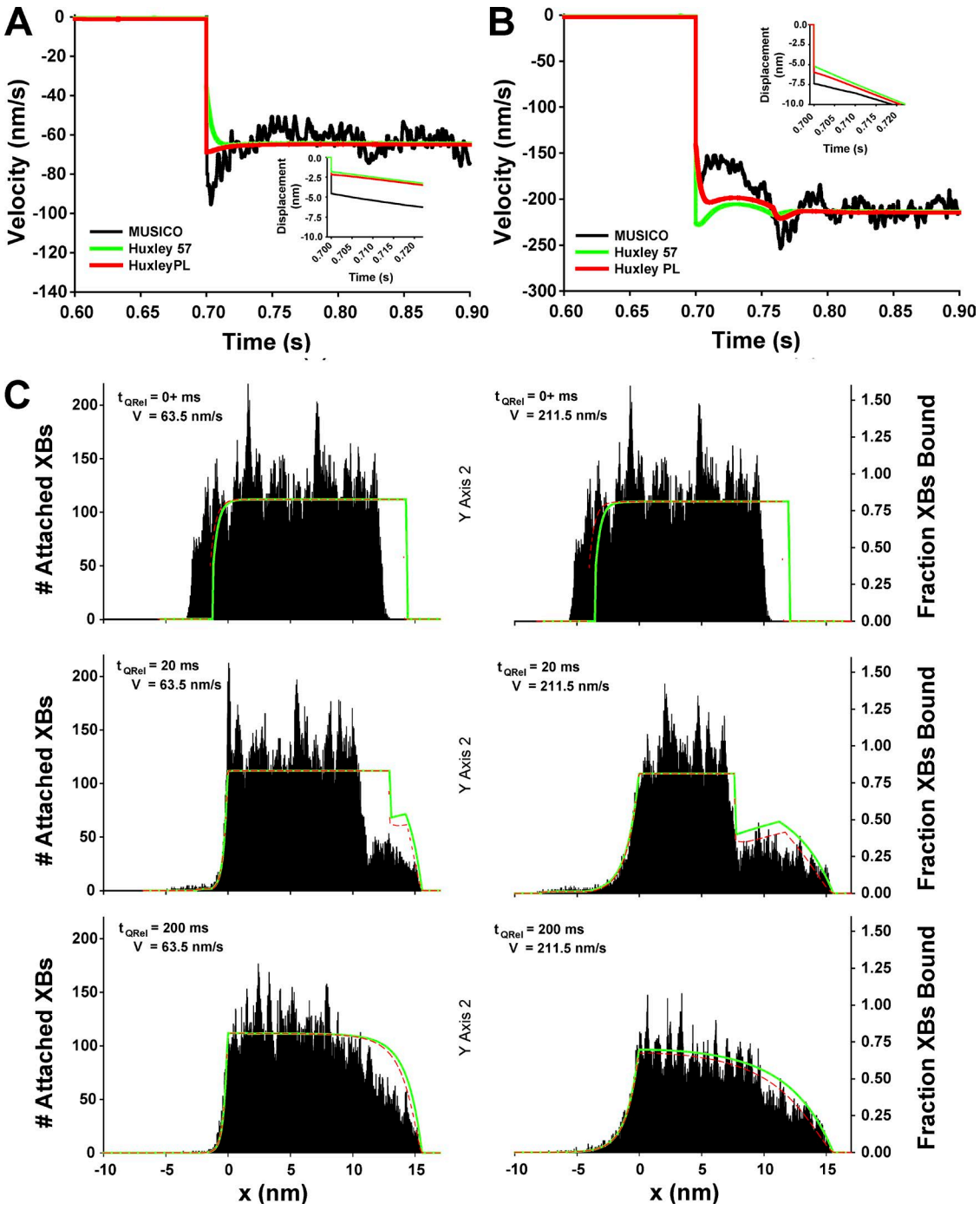

Figure S4. **Two-state model predictions of velocities and distributions for shortening velocities of 63.5 and 215.5 nm/s (i.e., 0.04 and 0.133 of v_{max}) that correspond to MUSICO velocities for $F/F_o = T/T_o = 0.6$ and 0.4, respectively.** (A) Evolution of velocities after a quick release to isotonic force to match the steady-state velocity predicted by MUSICO at $F/F_o = 0.6$ (black line), Huxley 1957 (green line), and Huxley PL (red line). The displacements after release are significantly different because the quick releases in Huxley and Huxley PL simulation models were different in order to match the steady-state velocities of all three models (inset). After an initial transient, the slopes of the force-displacement lines are about the same, reflecting the same steady-state velocities. (B) Velocity evolution after quick release to isotonic force to match steady-state velocity predicted by MUSICO at $F/F_o = 0.4$. (C) Cross-bridge distributions and state probability density distribution functions at times $t_{QRel} = 0_+$, 20, and 200 ms after release to achieve steady-state velocity of 63.5 nm/s (left column) and of 215.5 nm/s (right column).

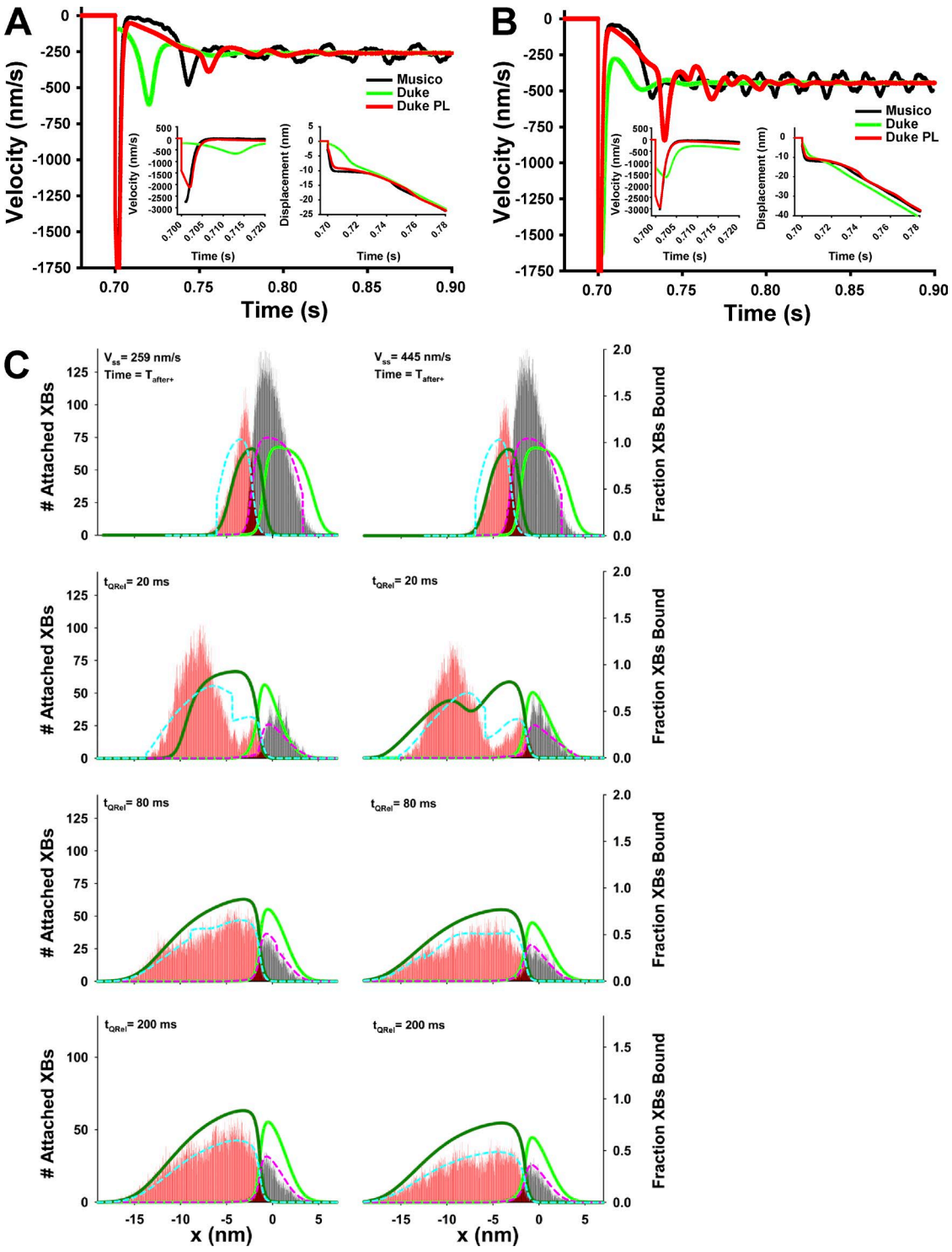

Figure S5. **Three-state model predictions of velocities and distributions for shortening velocity of 259 and 445 nm/s (i.e., 0.17 and 0.29 of v_{max}) that correspond to MUSICO velocities for F/F_o = T/T_o = 0.6 and 0.4, respectively.** (A) Evolution of velocities after a quick release to isotonic force to match the steady-state velocity predicted by MUSICO at F/F_o = 0.6 (black line), Duke (green line), and Duke PL (red line) models. The comparisons of early phase of velocity transients and the evolution of the displacements for all three models are shown as insets. (B) Velocity evolution after a quick release to isotonic force to match the steady-state velocity predicted by MUSICO at F/F_o = 0.4. (C) Cross-bridge distributions and state probability density distribution functions at times t_{QRel} = 0_+, 20, and 200 ms after the release to achieve steady-state velocity of 259 nm/s (left column) and of 445 nm/s (right column).

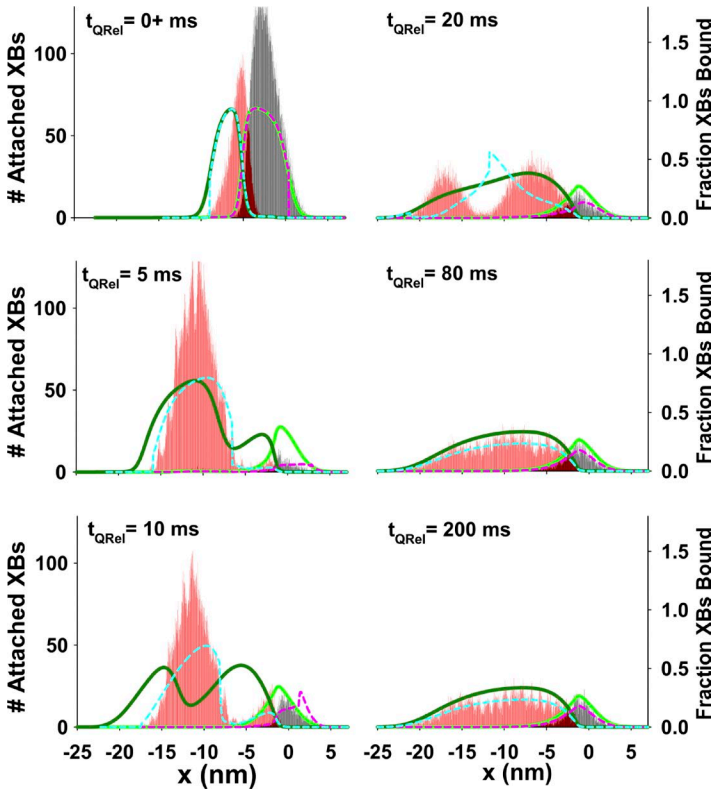

Figure S6. **The cross-bridge distributions t_{QRel} = 0+, 5, 10, 20, 80, and 200 ms after a quick release to zero isotonic load for model, where black bars represent weakly bound cross-bridges and red bars the post-power stroke bound myosins (MUSICO).** Duke state probability density distribution functions are shown as solid lines (weakly bound as a green line and post-power stroke a dark green line) and Duke PL as dashed lines (pink and cyan, respectively).

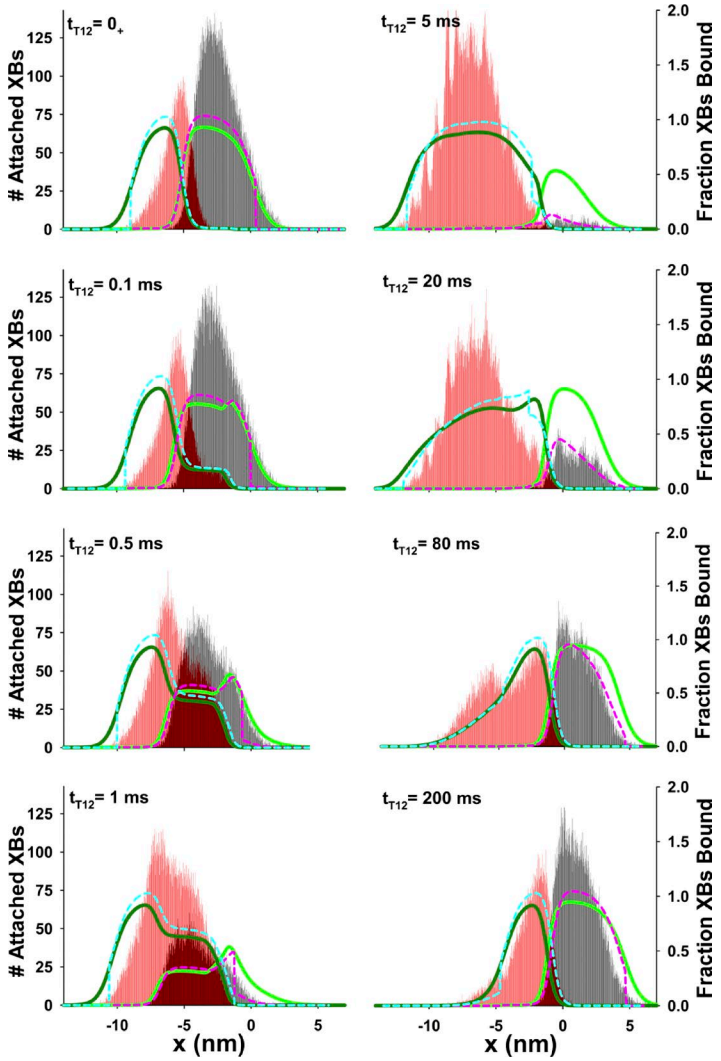

Figure S7. **Three-state model (Duke) predictions of the evolution of the cross-bridge distributions during $T_1 - T_2$ transitions after a quick decrease in length of 7.35 nm.** The bound cross-bridge distributions and state probability density distribution functions at times $t_{T_1T_2} = 0_+$, 0.1, 0.5, …, up to 200 ms after T_1 change of length. Duke state probability density distribution functions are shown as solid lines (weakly bound as a green line and post-power stroke a dark green line) and Duke PL as dashed lines (pink and cyan, respectively).

Table S1. **Values of key sarcomere lattice parameters**

Parameter	Symbol	Value
Sarcomere slack length		2.175 μm
Lattice interfilament distance[a]	d_{10}	37 nm
Myosin filament length[b]		∼1.58 μm
Number of crowns[b]		50
Crown spacing[b]		14.3 nm
Myosin radius	r_m	7.8 nm
Actin filament length[c]		∼1 μm
Number of actin monomers		364
Inter monomer spacing[d]		2.735 nm
A strand half period[d]		35.55 nm
Actin radius is r_a = 3.5	r_a	3.5 nm
Filament moduli (E × A)		
Actin[d,e]	K_a	0.65×10^5 pN
Myosin[d]	K_m	1.32×10^5 pN
Series elastic component (SE)		
SE Huxley 1957 and PL[f]	K_{SE}^{Hux}	144 pN/nm
SE Duke and PL[f]	K_{SE}^{Duke}	198 pN/nm

Model parameters used in this study are shown.
[a]Matsubara and Elliott (1972) and Millman (1998).
[b]Luther et al. (2008).
[c]Frog sartorius muscle Burgoyne et al. (2008).
[d]Huxley et al. (1994), Wakabayashi et al. (1994), and Prodanovic et al. (2016).
[e]Kojima et al. (1994).
[f]Chosen to match the filament elasticity from MUSICO.

Table S2. **Values of key cross-bridge kinetic parameters and constraints**

Parameter	Symbol	Value
Huxley 57 and PL parameters		
Myosin–actin binding rate	f	43.3 s^{-1}
Myosin detachment rate	g_1	10 s^{-1}
Myosin detachment rate 2	g_2	209 s^{-1}
Cross-bridge distortion displacement scale	h	15.6 nm
Piazzesi–Lombardi length of binding region $\mathscr{R}$	$\ell_{\mathscr{R}}$	15.6 nm
The Zahalak factor for $x \geq h_{Zah}$ = 15.6 nm[a]	f_{Zah}	1.8
Cross-bridge stiffness[a]	κ	0.58 pN/nm
Duke and Duke PL parameters		
Free energy gain	ΔG_{bind}	3 k_BT
	ΔG_{stroke}	15 k_BT
Myosin–actin binding rate[a]	k_{bind}	170 s^{-1}
Power stroke rate (cap at x_o = −1.5 nm)	k_{stroke}^{cap}	1,000 s^{-1}
ADP release/detachment rate[a]	k_{ADP}^{o}	56 s^{-1}
Power stroke[a]	d	10.6 nm
Second power stroke[a]	δ	0.9 nm
Piazzesi–Lombardi length of binding region $\mathscr{R}$[b]	$\ell_{\mathscr{R}}$	9.4 nm
Cross-bridge stiffness	κ	1.3 pN/nm
Duke and Duke PL original parameters		
Myosin–actin binding rate	k_{bind}	40 s^{-1}
Power stroke rate (cap at x_o = −1.5 nm)	k_{stroke}^{cap}	1,000 s^{-1}
ADP release/detachment rate	k_{ADP}^{o}	80 s^{-1}
Power stroke	d	11 nm
Second power stroke	δ	0.5 nm

Huxley 1957 parameters are taken from Huxley (1957), and Duke parameters are taken from Duke (1999) unless differently denoted.
[a]Chosen to match experimental data.
[b]Value chosen to provide responses close to MUSICO predictions.

REFERENCES

Burgoyne, T., F. Muhamad, and P.K. Luther. 2008. Visualization of cardiac muscle thin filaments and measurement of their lengths by electron tomography. *Cardiovasc. Res.* 77:707–712. http://dx.doi.org/10.1093/cvr/cvm117

Duke, T.A. 1999. Molecular model of muscle contraction. *Proc. Natl. Acad. Sci. USA.* 96:2770–2775. http://dx.doi.org/10.1073/pnas.96.6.2770

Huxley, A.F. 1957. Muscle structure and theories of contraction. *Prog. Biophys. Biophys. Chem.* 7:255–318.
Huxley, H.E., A. Stewart, H. Sosa, and T. Irving. 1994. X-ray diffraction measurements of the extensibility of actin and myosin filaments in contracting muscle. *Biophys. J.* 67:2411–2421. http://dx.doi.org/10.1016/S0006-3495(94)80728-3
Kojima, H., A. Ishijima, and T. Yanagida. 1994. Direct measurement of stiffness of single actin filaments with and without tropomyosin by in vitro nanomanipulation. *Proc. Natl. Acad. Sci. USA*. 91:12962–12966. http://dx.doi.org/10.1073/pnas.91.26.12962
Luther, P.K., P.M. Bennett, C. Knupp, R. Craig, R. Padrón, S.P. Harris, J. Patel, and R.L. Moss. 2008. Understanding the organisation and role of myosin binding protein C in normal striated muscle by comparison with MyBP-C knockout cardiac muscle. *J. Mol. Biol.* 384:60–72. http://dx.doi.org/10.1016/j.jmb.2008.09.013
Matsubara, I., and G.F. Elliott. 1972. X-ray diffraction studies on skinned single fibres of frog skeletal muscle. *J. Mol. Biol.* 72:657–669. http://dx.doi.org/10.1016/0022-2836(72)90183-0
Millman, B.M. 1998. The filament lattice of striated muscle. *Physiol. Rev.* 78:359–391.
Prodanovic, M., T.C. Irving, and S.M. Mijailovich. 2016. X-ray diffraction from nonuniformly stretched helical molecules. *J. Appl. Cryst.* 49:784–797. http://dx.doi.org/10.1107/S1600576716003757
Wakabayashi, K., Y. Sugimoto, H. Tanaka, Y. Ueno, Y. Takezawa, and Y. Amemiya. 1994. X-ray diffraction evidence for the extensibility of actin and myosin filaments during muscle contraction. *Biophys. J.* 67:2422–2435. http://dx.doi.org/10.1016/S0006-3495(94)80729-5